Blast vibration modeling using linear superposition method

H. Mansouri[*] and M.A. Ebrahimi Farsangi

Mining Engineering Department, Shahid Bahonar University of Kerman, Kerman, Iran

Abstract

A linear superposition method was used for modeling the time history of the production blast vibrations and optimizing the blast sequence to reduce vibration levels in Sar-Cheshmeh copper mine, Kerman, Iran. A single-hole blast for modeling and two double-hole blasts with time delays of 25 and 65 ms between two holes for modeling validation were carried out. The generated vibrations were measured at seven points with different distances and directions around the blasts. These records contain information about the complex mechanism of seismic energy radiation from an explosive source as well as the filtering effect of the signal travel path. Totally, 40 seismograms were synthesized (3 components for each point) for two blasts using the linear superposition method. The results obtained presented a good correlation between the synthetic and measured seismograms. Also, a comparison was made between the measured peak particle velocities (PPVs) and those obtained from the scaled-distance method and linear superposition modeling. This shows the merits of linear superposition modeling to predict PPVs. Moreover, the recorded seismograms of the single-hole blast were used to simulate the vibrations produced by a production blast at seven points. Furthermore, by using a systematic variation of firing delay in the modeling procedure, the effect of delay on the production blast vibrations was studied. The production blast simulations showed that for Sar-Cheshmeh copper mine, the blasts carried out with the inter-row delays more than 40 ms can significantly reduce vibration levels.

Keywords: *Vibration Simulation, Linear Superposition Method, Peak Particle Velocity (PPV), Sar-Cheshmeh Copper Mine.*

1. Introduction

Blast vibrations are undesirable phenomena in the surface and underground mining, that may repeatedly trouble the mining industry. The blast vibrations from these mines may be detrimental to the environment when there is population in the vicinity. Several methods such as the empirical, artificial intelligence, and numerical methods are currently known, which allow the prediction of ground vibrations caused by mine blasting operations [1-23]. Perhaps, the most widely used method is the so-called "scaled-distance" one, which is based on the empirical principle that states: "The vibration level at a point is inversely proportional to the distance from the blast, and is directly proportional to the blast charge". Many different empirical relations have been introduced between the charge weight, distance from the source, and the peak particle velocity (PPV) [2-4, 6-9, 12, 13]. All of these relations were determined using regression method on the measured PPV and scaled-distance data. In order to have valid results, there should be a good correlation between the PPV and scaled-distance data. The parameter defining the correlation quality is the correlation coefficient, which must be more than 0.7 for considering the results as valid [24]. The geological and geotechnical properties, explosive type, and blast geometry have not yet been incorporated into this type of relations [24, 25]. Since the number of influencing parameters is high, the artificial neural networks (ANNs) and several artificial intelligent methods (AIMs) have been developed to predict the rock blasting vibrations. Many researchers have used

ANN and support vector machines to estimate the PPV and air blast [16- 19, 21, 22, 26, 27]. The empirical and AIM methods only provide an estimation of the maximum amplitude of particle velocity, and give no information about the complete seismic waveform. Also, the propagation of blast-induced ground vibration was studied using numerical method [28].

Using the linear superposition method, a complete seismic waveform produced by a production blast may be modeled, and the weaknesses of the empirical and AIM methods can be overcome.

The linear superposition method was used and validated by Anderson [29] and Hinzen [25]. In the Hinzen's work, after explaining the principles of this method, it was validated by carrying out a five-hole production blast and measuring blast vibrations at two points.

In the present work, in addition to the validation of linear superposition method with more blasts, the effects of medium and distance from the blast on the simulation results were studied. Furthermore, the validity of the linearity or non-linearity of blast vibration superposition with distance from the blast was examined. Moreover, the simulated seismograms were used to predict PPV at a given point around the blast, and the results were compared to the results obtained from the scaled-distance method.

2. Linear superposition modeling

During the past several years, various techniques have been developed for calculating the theoretical seismograms that model the complete seismic waveform radiated by a single-hole blast [30, 31]. In these techniques, the source of seismic energy and the medium of wave propagation have to be known, which are not fulfilled in the case of the blast vibration. To overcome these difficulties, the linear superposition method was developed, which is a combination of the field measurements and computer simulations [25]. This method is based on the principle that the seismogram measured at a given point is the result of the linear superposition of the seismograms in time domain, emitted by every one of the single-hole charges. The principle of linear superposition of vibration has been studied by Stump and Reinke [32] to predict vibration waveform radiated from a single column of explosives, and to predict the total vibration from a full-scale blast. Blair [33] has studied the linearity and non-linearity models for blast vibration, and has concluded that around a blast hole, two schemes, linear superposition and non-linear superposition, may exist. For a blast

with widely spaced blast holes, monitored in the far field, the linear superposition model is valid, whereas in a blast in which the blast holes are virtually coalesced and monitored in the near field, the non-linear superposition model is valid [33].

Due to the linearity of the problem and the principle of the linear superposition method, in which the distributed sources can be described as the sum of the multiple point sources, there is no additional difficulty in modeling even a very complicated source. In addition to the spectral amplitudes, all phase effects from the superposition are included in the synthetic seismogram. The phase effects are a crucial point in optimizing the firing times. By changing the delay time between two successive detonations, the signal compositions can be modified and thus the maximum amplitude and pseudo-frequency of the resultant signal change. The part of the solution that connects the force distribution at the source with the displacements at the receiver is termed the elasto-dynamic Green's function. Derivation of the Green's function is the key step to the synthetic seismogram calculations. This function must take into account the elastic properties of the materials and the appropriate boundary conditions [34].

The Green's function $G(x, t)$ gives the displacement at point x that results from the unit force function applied at point x_0 [35].

$$u_i(x,t) = G_{ij}(x,t; x_0, t_0) f_j(x_0,t_0) \qquad (1)$$

Equation 1 gives the displacement u from a realistic source with the force vector, or source time function f, of a blast row, synthesized using the displacement produced by the simplest possible source. It is a uni-directional unit impulse, precisely in space and time. The ground velocity can be achieved by a differentiation of Equation 1. If the displacement field of the blast row is a linear superposition of the displacements produced by the individual holes of the blast pattern, the source function can be separated into two parts (ignoring the mathematical dependencies of x, x_0, t, and t_0), as follows:

$$F = f_s * f_R, \qquad (2)$$
$$f_R = a_i\delta(t-t_i), \quad i = 1\ldots N \qquad (3)$$

where
N = number of charges,
t_i = firing time of charge i
In the above formulas, the shape of the measured parameter (displacement or velocity) is assumed

to be identical for all individual holes. The term *fs* is the source time function of a single hole, f_R is an impulse series, and δ is the delta function. The superposition of the individual signals is mathematically expressed as a convolution. The convolution with a delta function leaves the original function unchanged. The delta function may act to produce a time shift in the original time series. The amplitudes of the impulses a_i in Equation 3 are scaling factor for the seismic effects of the individual holes. The arriving times of the body waves from detonation of the individual holes at the observation point are expressed by the position of the impulse in the series. The displacement time history from a single blast at a specific location can be written as:

$$u_s = f_s * G \tag{4}$$

The displacement time history can be measured at a field test. Combining Equations 1 and 2, the displacement of a complete row can be obtained, as follows:

$$U = f_s * f_R * G \tag{5}$$

The convolution is commutative and associative, then,

$$U = f_s * G * f_R \tag{6}$$

$$U = u_s * f_R \tag{7}$$

The impulse series f_R can be calculated, and the convolution in Equation 7 combines the field measurement and computer simulation. Using Equation 7 and measurements of the single-hole motions, the ground motions of a production blast can be calculated without calling the Green's function. The procedure starts by drilling a single hole and loading it by a charge similar to the holes of actual blast. The displacement or velocity time history is then measured at locations, for which the ground vibrations are to be predicated or reduced. The next step is the calculation of the impulse series for each geophone position. These series are convolved with u_s to simulate the complete blast seismogram at the specific locations [35].

Also, the effect of delay time between two successive detonations on PPV can be modeled.

3. Sar-Cheshmeh copper mine

Sar-Cheshmeh copper mine, as one of the largest open-pit copper mines in the world, with a production of 60000 ton/day, is located in 55 km south of Rafsanjan, Kerman, Iran (Figure 1). It extends on an area of 1700×2900 m^2, with a cut-off grade of 0.25%. Due to the presence of diverse geological structures and different types of rock alteration in Sar Cheshmeh region, the rock mass is very heterogeneous. There are two principal mineralized rock types, Andesit (host-rock) and Sar-Cheshmeh Porphyry (intrusive). The deposit was crossed by the dykes, which play a fundamental role in the behavior of the rock mass (Figure 2).
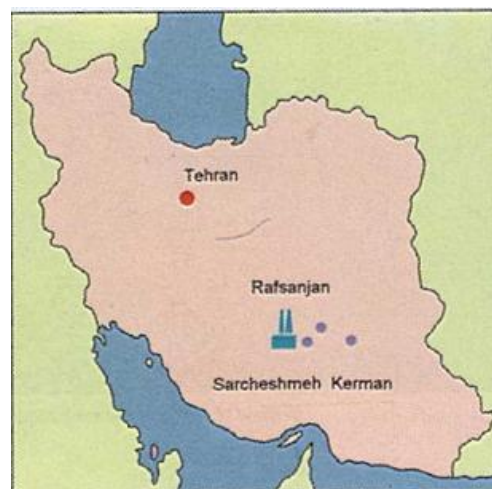

Figure 1. Location of Sar-Cheshmeh copper mine.

Some parts of the mine, in particular, the west wall, face a critical stability problem. This is controlled by large geological structures (dykes and major faults) and unfavorable hydro-geological conditions. It is likely to be more worsened by the deepening of the pit from 300 to 800 m (based on the expansion plan) [29]. Under such a condition, the production blasts, carried out in the vicinity of the pit wall, can contribute to worsen the mine stability.

The production blasts are carried out under a wet condition, and the explosive used is emulsion (Emulan). For production blasting in Sar Cheshmeh copper mine, hole diameter, bench height, stemming, and sub-drilling are 251 mm, 12.5 m, 8 m, and 3.5 m, respectively. The blasting patterns 7 m × 9 m, 7.5 m × 9.5 m, and 8 m ×10 m are being used.
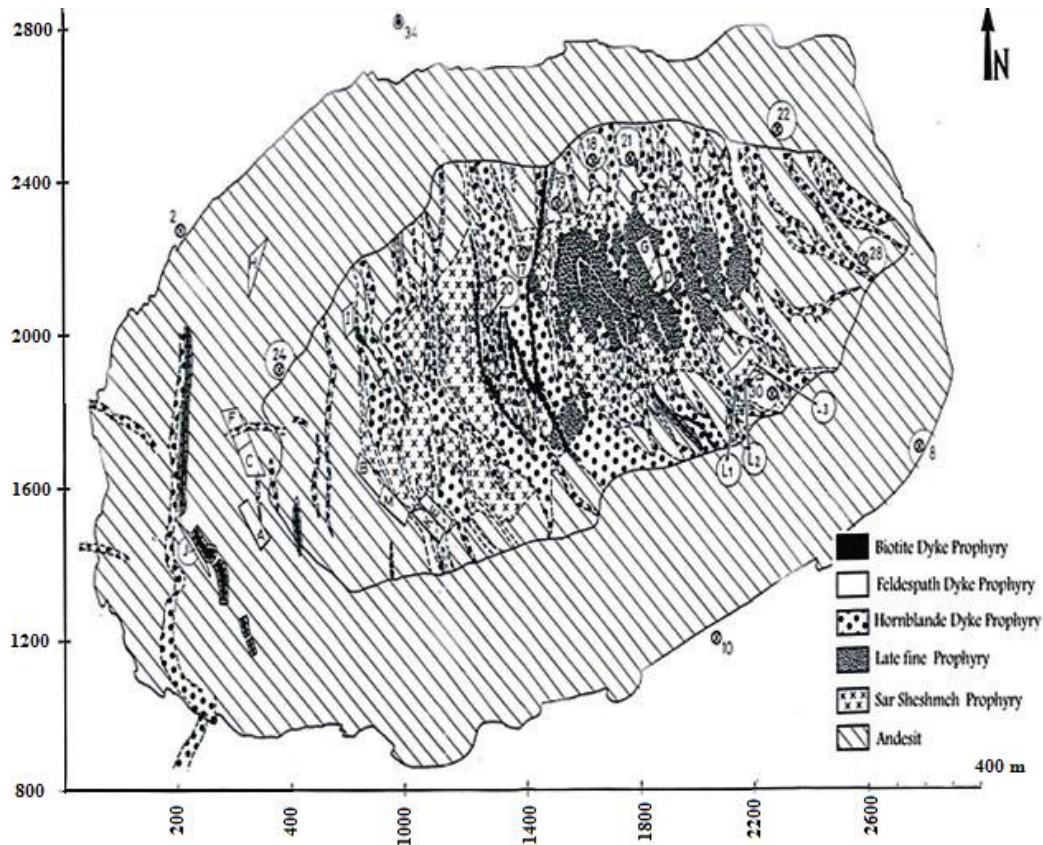
Figure 2. Sar-Cheshmeh copper mine deposit locations of blasts L1, L2, and L3, and measuring points [36].

4. Linear superposition method validation

Field tests were carried out to verify the validation of the linear superposition method. Two steps were involved in the validation process.

In the first step, one single-hole blast (L1) and two double-hole blasts (L2 and L3) were carried out, and the vibrations were measured at seven points with different distances fromblast hole. Total charges of blasts L1, L2 and L3 were 350, 700, and 700 kg, respectively. Charge per delay for the blasts L2 and L3 was 350 kg. Delay time between two holes for the blast L2 was 65 ms and that for the blast L3 was 25 ms. As these three test blasts were in the neighboring of each other, and the measuring points are common, the wave propagation media and the distances between every measuring point and three test blasts are the same. The plan presented in Figure 2 shows the positions of seven measuring points (2, 8, 10, 21, 22, 24, and 36) and three blasts.

In the second step, the seismograms of blasts L2 and L3 in different measuring points were simulated by the linear superposition method using the single blast of L1 signal. Totally, 40 seismograms were synthesized (three seismograms for each point) for two tests. These

seismograms were compared with the measured ones.

4.1. Validation results analysis
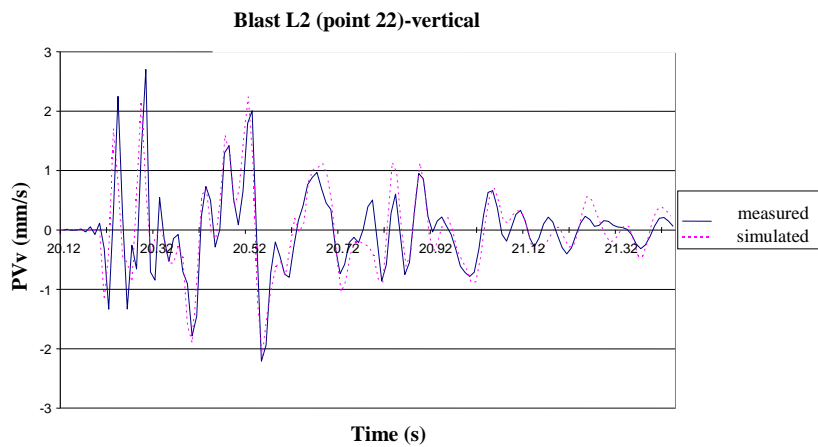### 4.1.1. Analysis of time history and frequency spectrum

With three blasts L1, L2, and L3 and seven measuring points, totally 61 records were obtained (out of 63 records expected, 2 were omitted due to high noises). The time history records of L1 were used to simulate 21 time history seismograms for the blast L2 and 21 time history seismograms for the blast L3. These seismograms were compared with the measured data. Also the synthetic and measured frequency spectra were compared for the blasts L2 and L3.

Due to the space limitation, out of 40 synthetic seismograms, only the results of simulation at point 22 for three components of the blast L2 are presented. For the rest, only the simulation results of the longitudinal components for the blasts L2 and L3 at different points are presented.
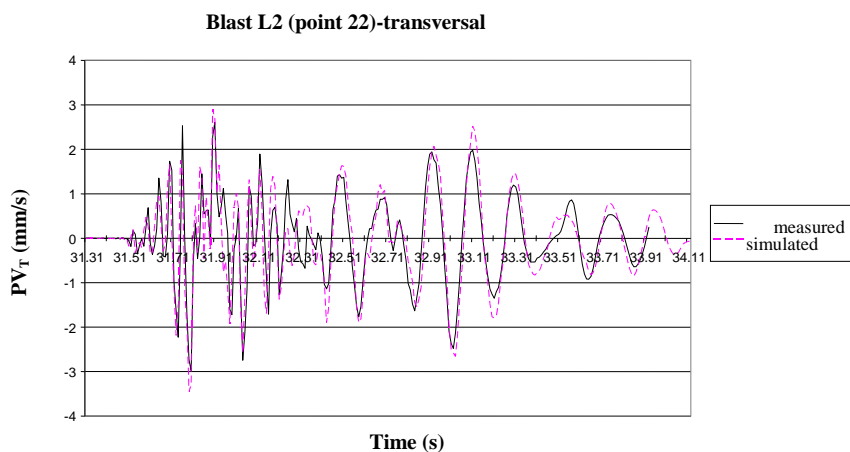
Figure 3 shows three components of the measured and synthetic seismograms at point 22 at a distance of 661 m from the blast L2. As it can be seen in this figure, the general forms of the measured and simulated signals are similar.

Blast L2 (point 22)-longitudinal

(a)

Blast L2 (point 22)-vertical


**(b)**

Blast L2 (point 22)-transversal
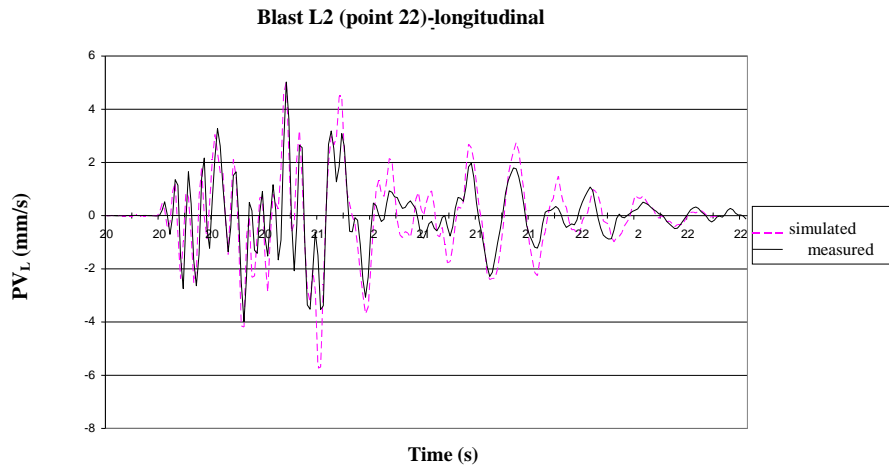
(c)

Figure 3. Comparison of measured and synthetic seismograms for blast L2 at point 22. (a) longitudinal component; (b) vertical component; (c) transversal component.

Figures 4 and 5 give the longitudinal components of measured and synthetic seismograms at points 2, 8, 21, 24, and 34 (longitudinal component at point 10 had noise, and thus was not used) for blasts L2 and L3 respectively. As it can be seen,

the measured seismograms and the simulated ones fit fairly well even at large distances. The good fitness between the measured and simulated seismograms confirms the presumption of a linear superposition of single hole wavelet.
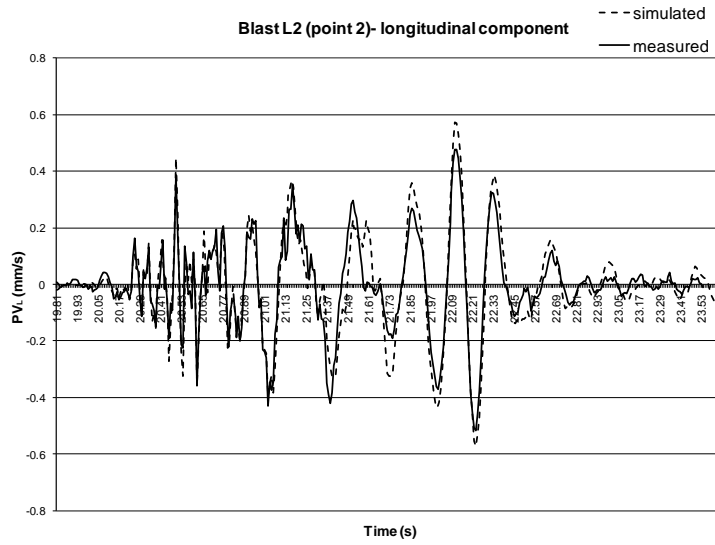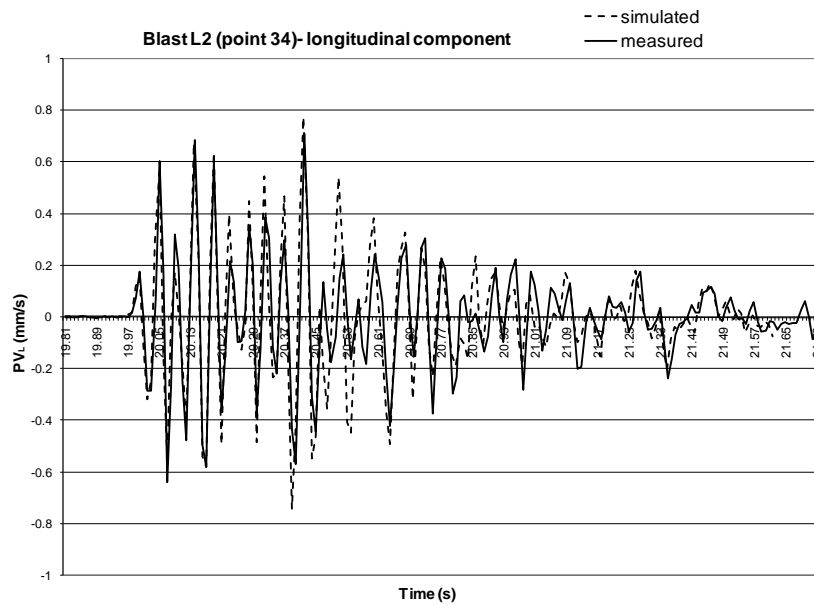
(a)
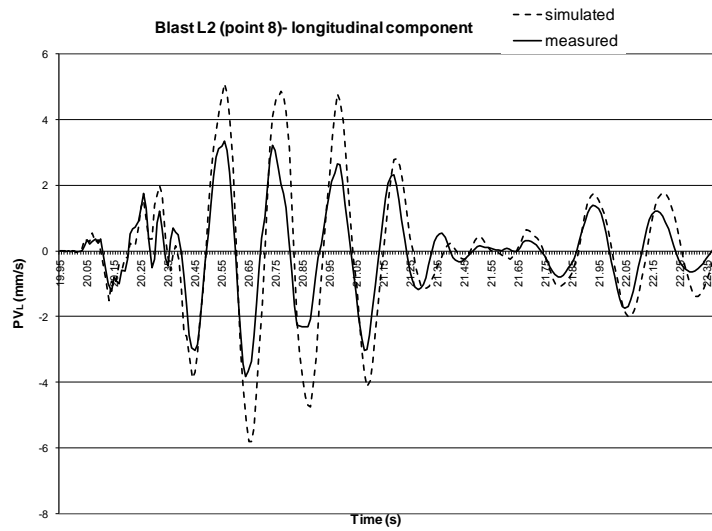
(b)
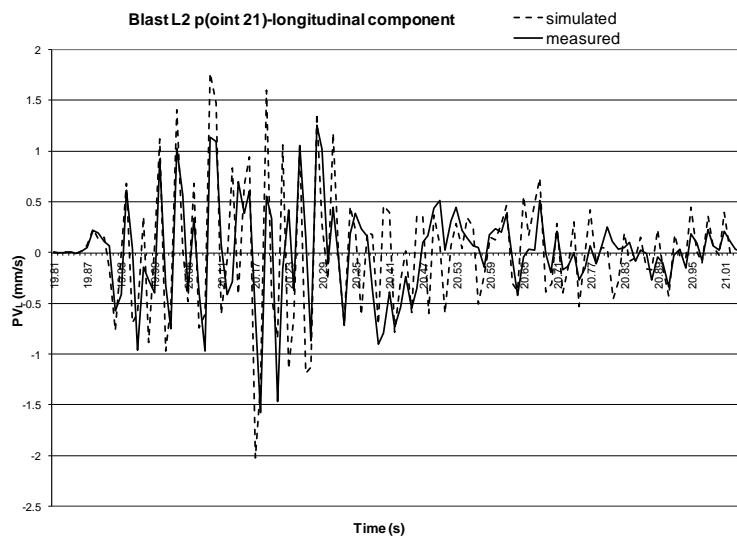
(c)

Figure 4. Measured and synthetic seismograms of blast L2 at points (a) 2, (b) 8, (c) 21, (d) 24, and (e) 34 (longitudinal component).
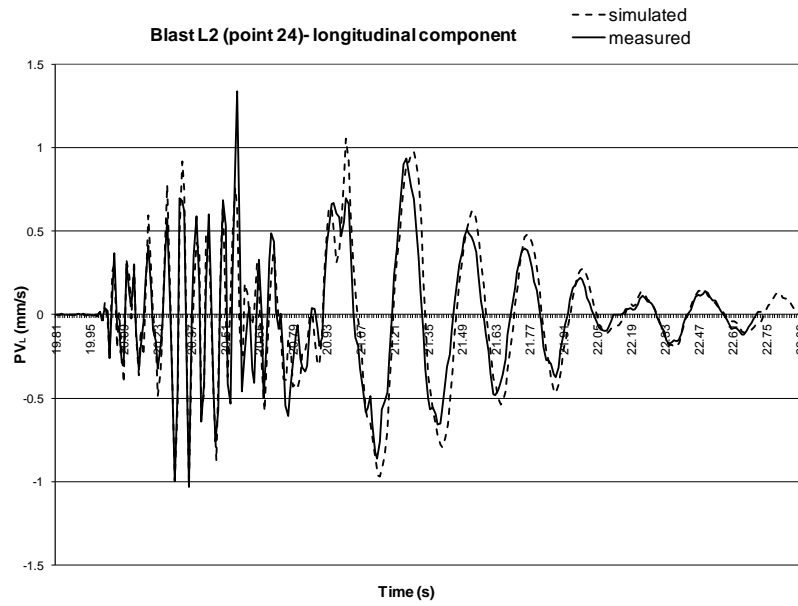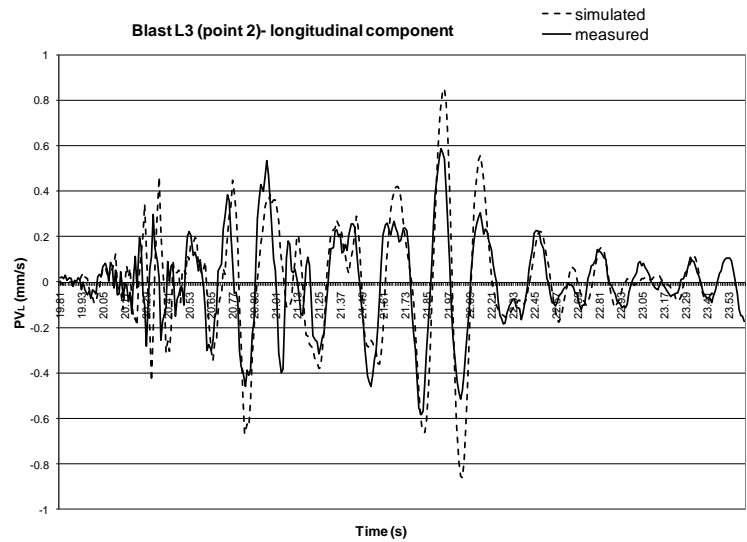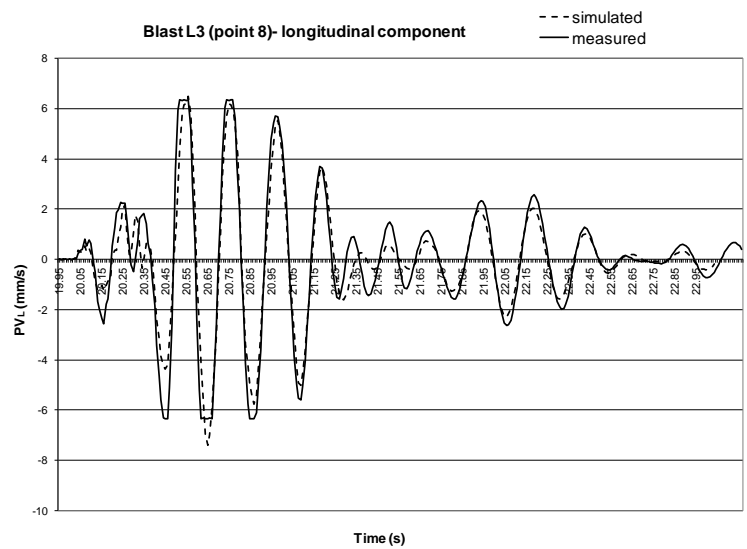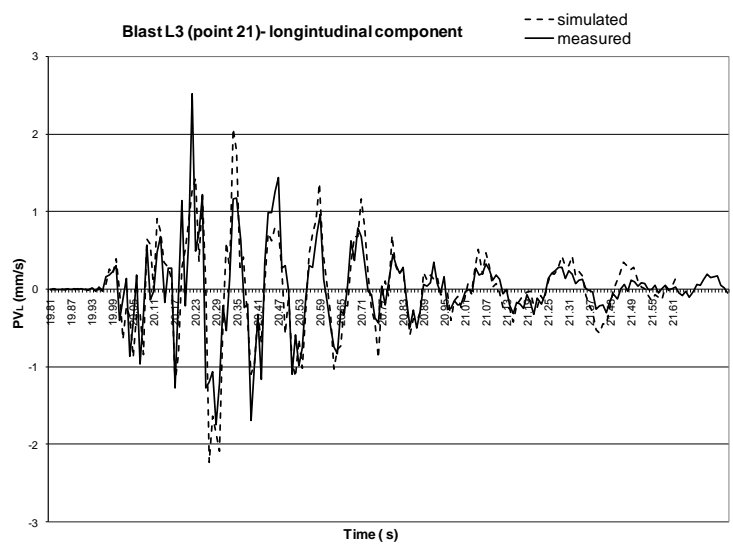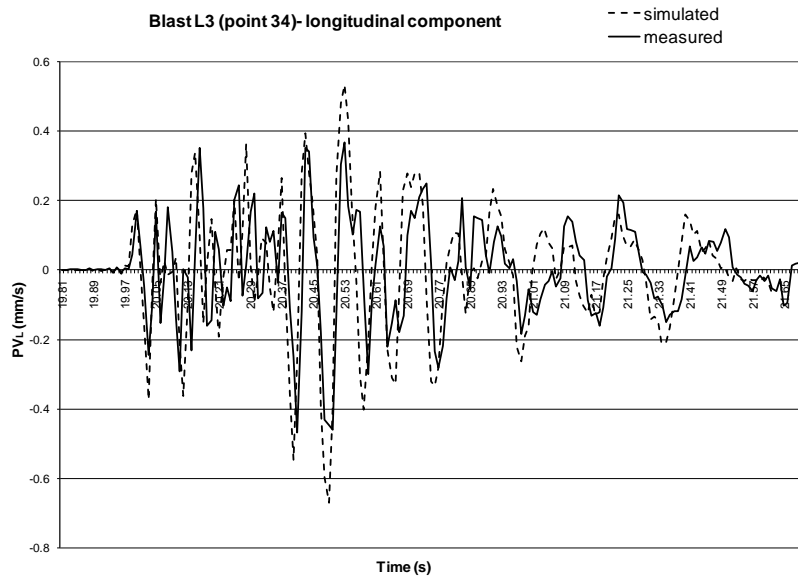
(d)
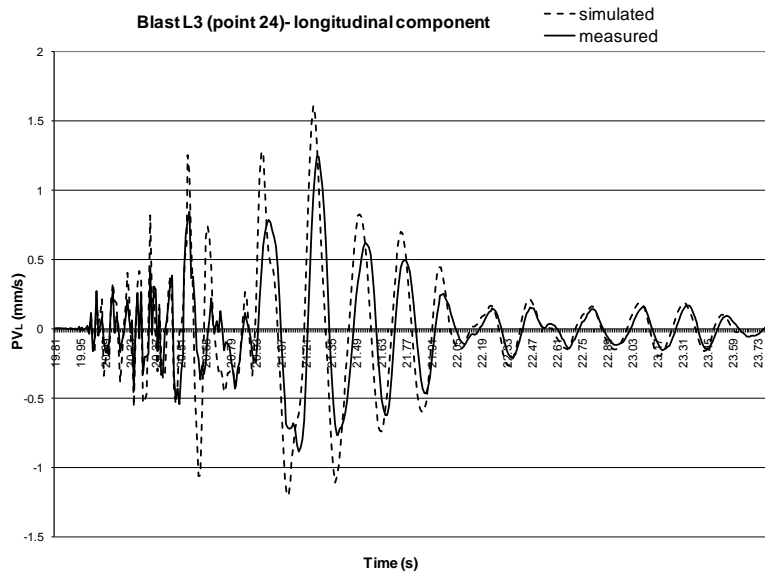

(e)
Figure 4. Continued.

(a)

(b)

(c)

Figure 5. Measured and synthetic seismograms of blast L3 at points (a) 2, (b) 8, (c) 21, (d) 24, and (e) 34 (longitudinal component).

(d)

(e)
Figure 5. Continued.

Concerning the frequency contents of the measured and synthetic seismograms, Fourier amplitude spectra of them were compared. As examples, the Fourier amplitude spectra of measured and synthetic seismograms at point 22

for three components are shown in Figure 6. As it can be observed in this Figure, there are strong agreements between the simulated and measured frequency spectra.
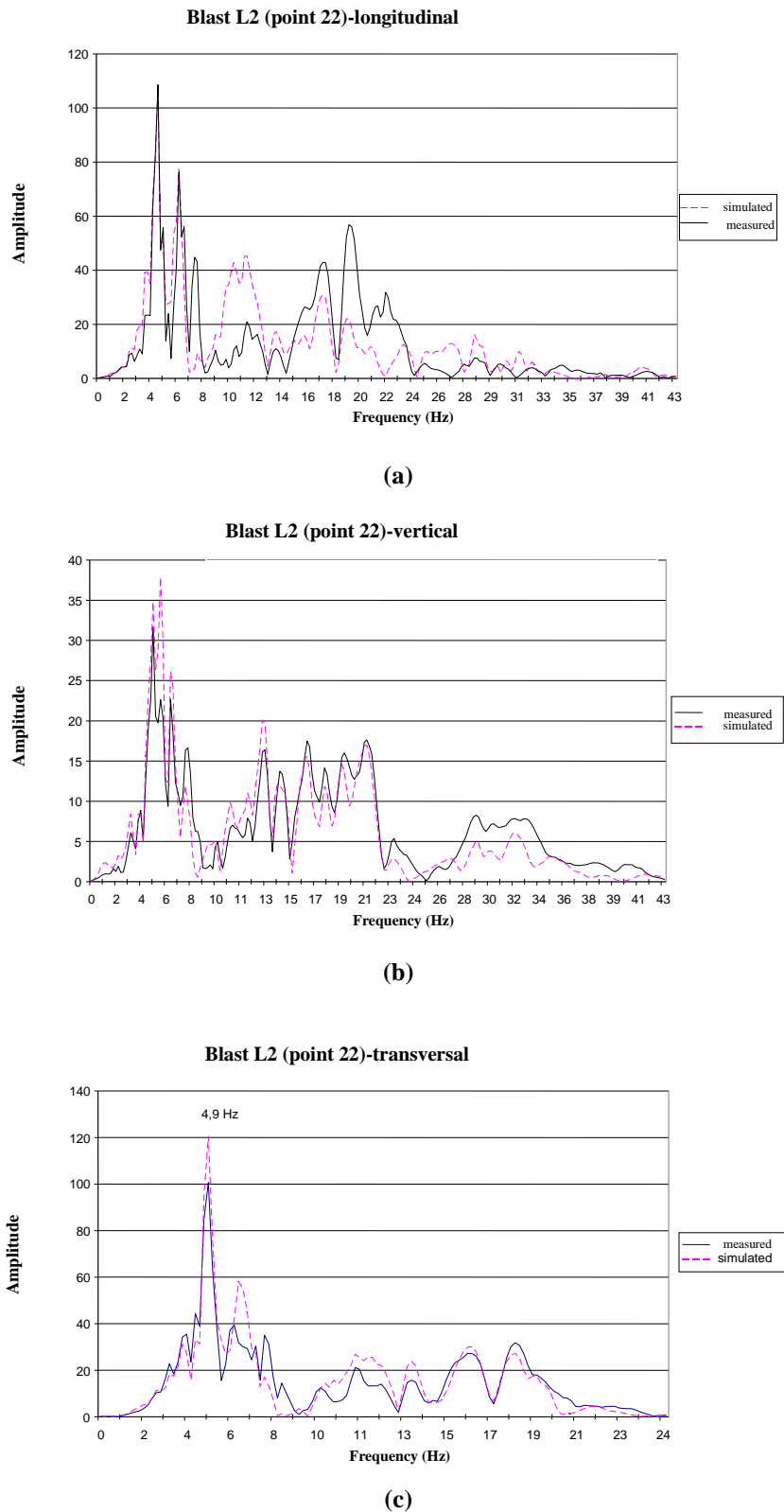
(a)

(b)

(c)

Figure 6. Measured and synthetic seismograms spectra of blast L2 at point 22. (a) longitudinal component, (b) vertical component, and (c) transversal component.

4.1.2. Analysis of peak particle velocity and peak frequency

To make a quantitative comparison between the measured and synthetic data, the differences between PPVs and peak frequencies of measured and simulated signals were calculated, as shown in Tables 1 and 2 for the blasts L2 and L3 respectively.

134

Table 1. Differences between PPVs and peak frequencies of synthetic and measured seismograms for three components of blast L2.

Differences*(%) \ Point	8	10	24	22	2	34	21
PPV_L	51	-	-10	5	6	4	3
PPV_V	6	1	-4	-18	13	-4	3
PPV_T	3	-3	-3	17	3	19	15
f_L	9	0	5	7	4	0	6
f_V	8	2	3	4	23	1	2
f_T	5	0	7	4	5	-40	-5

*(PPVmeasured-PPVsynthetic/PPVmeasured) × 100 or (fmeasured-fsynthetic/fmeasured) × 100

Table 2. Differences between PPVs and peak frequencies of synthetic and measured seismograms for three components of blast L3.

Differences* (%) \ Point	8	10	24	22	2	34	21
PPV_L	0	-	20	27	35	42	13
PPV_V	11	31	17	34	0	36	-13
PPV_T	40	35	43	13	7	7	2
f_L	9	0	5	7	4	0	6
f_V	2	5	54	16	5	3	8
f_T	5	12	2	4	5	0	-8

*(PPVmeasured-PPVsynthetic/PPVmeasured) ×100 or (fmeasured-fsynthetic/fmeasured) ×100

Based on the analysis carried out above, the following points can be remarked:

• The difference between the measured and calculated PPVs at various points varies from 0 to 51% for the blast L2. The difference 51% is related to the longitudinal component of point 8 that represents only 5% of the measures. 95% of PPVs show the differences less than 19%, while 71% of them present the differences less than 10%. For the blast L3, the measured and simulated PPVs have the differences varying from 0 to 43%. The mean observed difference is 9% for the blast L2 and 20% for the blast L3.

• The majority of the synthetic signals for the blasts L2 and L3 have amplitudes more than those for the measured signals.

• It can be observed that the differences between the measured and calculated peak frequencies vary from 0 to 40% for blast L2.

The differences are often less than 10% (90% of the cases observed). For the blast L3, 81% of the cases observed show a difference less than 10% between the measured and calculated peak frequencies.

• As shown in Figures 7 and 8, no correlation can be observed between the distance and the difference between PPVs of measured and simulated for the blasts L2 and L3.

• The results obtained show that the simulated blast L3 over evaluates PPV and peak frequency more than the simulated blast L2. This difference is probably due to their geological media. The blasts L2 and L1 (single hole) are situated in Andesit but two holes of blast L3 are located one in Andesit and the other in dyke. In this case, the blast L3 parameters are not perfectly identical to those for blast L1.
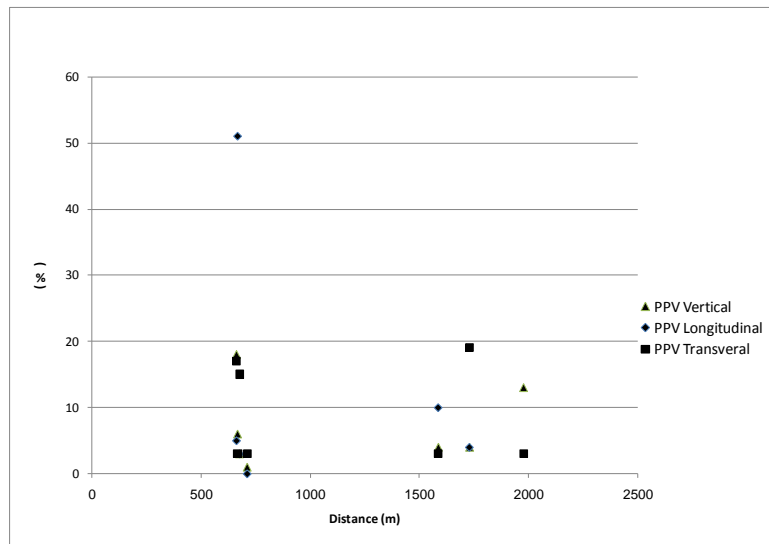
Figure 7. Percentage of differences between PPVs of synthetic and measured seismograms *vs*. distance from blast for blast L2.
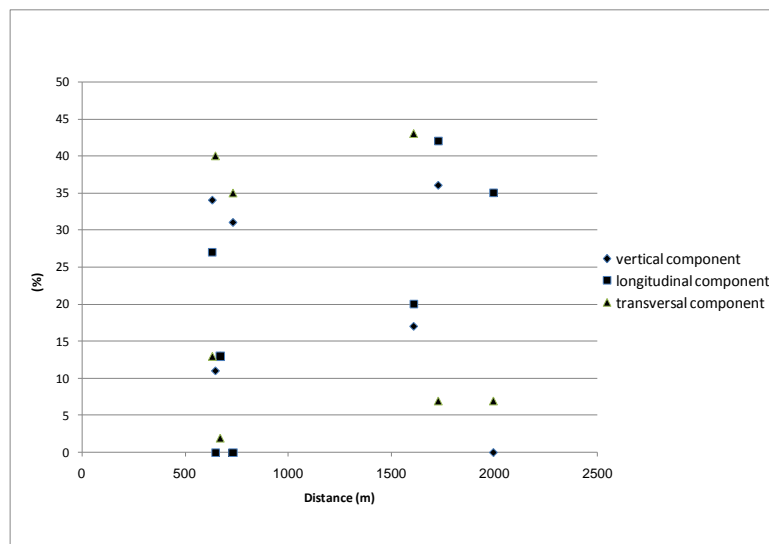

Figure 8. Percentage of differences between PPVs of synthetic and measured seismograms *vs*. distance from blast for blast L3.

5. Comparison between linear superposition method and scaled-distance method to predict PPV

A comparison was made between the scaled-distance method as the most widely used one, and the linear superposition method to evaluate PPVs. In the first step, 12 production blasts (blasts A to K and M in Figure 2) were carried out and PPVs were measured at different points (59 points) and 177 records were obtained. In the second step, for three components, the attenuation laws based on the scaled-distance were derived for Sar Cheshmeh copper mine, which are as follow [36]:

$PPV_L = 176.29(D/(Q)^{0.5})^{-1.1976}$
$PPV_V = 107.56(D/(Q)^{0.5})^{-1.1479}$
$PPV_T = 144.84(D/(Q)^{0.5})^{-1.1692}$

where

D = distance from blast (m)
Q = charge per delay (kg)
In the third step, based on the scaled-distance relations obtained for Sar Cheshmeh copper mine, PPVs for the blasts L2 and L3 at different measuring points were estimated. Charge per delay was 350 kg and the distances from two blasts for different points are as indicated in Table 3.

The comparisons made between the measured and estimated PPVs by linear superposition and scaled-distance methods for seven measuring points around the blasts L2 and L3 are shown in Tables 4 and 5, respectively. As it can be seen in these tables, from 40 values of PPVs predicted, in 32 cases, the linear superposition method was more accurate than the scaled-distance method.

Table 3. Distance of different measuring points from blasts L2 and L3.

Measuring point	22	8	21	10	24	34	2
Distance from blast L2 (m)	661	666	675	710	1585	1728	1975
Distance from blast L3 (m)	635	650	673	735	1610	1729	1996

Table 4. Comparison between measured and estimated PPVs by linear superposition method and scaled-distance method for blast L2.

Point	22	8	21	10	24	34	2
PPV_L measured (mm/s)	**5.02**	**-3.83**	**-1.57**	-	**1.34**	**0.70**	-0.52
PPV_L estimated by linear superposition method (mm/s)	**-5.30**	-5.8	**2.00**	-	**1.20**	**0.73**	0.55
PPV_L estimated by scaled-distance method (mm/s)	2.47	**2.45**	2.40	-	0.87	0.78	0.67
PPV_V measured (mm/s)	**2.70**	-2.13	-1.55	1.88	0.73	0.78	-0.31
PPV_V estimated by linear superposition method (mm/s)	**2.70**	2.26	1.6	1.90	0.70	0.75	-0.35
PPV_V estimated by scaled-distance method (mm/s)	1.80	1.78	1.75	1.65	0.66	0.60	0.51
PPV_T measured (mm/s)	-2.98	4.87	1.09	-2.17	-1.14	0.42	-0.63
PPV_T estimated by linear superposition method (mm/s)	-3.50	5.00	-1.25	2.10	1.10	0.50	-0.65
PPV_T estimated by scaled-distance method (mm/s)	2.24	2.22	2.18	2.06	0.80	0.73	**0.62**

Two near values in each cell were bolded. Sub-scriptionsL, V, and T refer to longitudinal, vertical, and transversal components, respectively.

Table 5. Comparison between measured and estimated PPVs by linear superposition method and scaled-distance method for blast L3.

| Point	22	8	21	10	24	34	2
PPV_L measured (mm/s)	**-6.14**	**6.35**	**2.52**	-	1.25	-0.47	**0.59**
PPV_L estimated by linear superposition method (mm/s)	**7.8**	**6.35**	**-2.55**	-	**1.50**	**0.67**	0.80
PPV_L estimated by scaled-distance method (mm/s)	2.59	2.52	2.41	-	0.85	0.78	**0.66**
PPV_V measured (mm/s)	**2.23**	4.86	4.21	-1.60	0.60	-0.33	0.44
PPV_V estimated by linear superposition method (mm/s)	3.00	5.38	3.64	2.10	-0.70	0.45	-0.44
PPV_V estimated by scaled-distance method (mm/s)	**1.88**	1.83	1.76	2.59	**0.65**	0.60	0.50
PPV_T measured (mm/s)	-4.52	-6.35	-2.16	2.15	-0.84	0.74	-0.75
PPV_T estimated by linear superposition method (mm/s)	-5.10	8.9	-2.2	2.90	-1.20	0.79	**0.80**
PPV_T estimated by scaled-distance method (mm/s)	2.35	2.29	2.2	**1.98**	0.79	0.73	0.62

Two near values in each cell were bolded.

6. Simulation of production blasts

In order to estimate PPVs and study the relation between the blast sequence and PPVs for a production blast, ten production blasts were modeled. Each blast consists of 40 holes in five rows (a typical pattern in Sar-Cheshmeh copper mine), which were simulated based on the single-hole blast, L1, measured at seven points. For ten blasts, various delays between the rows were used, from 10 to 100 ms, and their effects on the vibration level were analyzed. For example, the synthetic waveforms for a production blast obtained at point 8 with a delay of 60 ms between the rows and a distance of 660 m from the blast are presented in Figure 9. As shown in this figure, the maximum PPVs that can be expected for the vertical, longitudinal, and transversal components are 22.2, 52.84, and 45.3 mm/s, respectively. The peak vector sum for this blast at point 8 was 60 mm/s. The maximum PPVs obtained at the other points were certainly not the same, depending on the distance from the blast and direction of the measuring point. The effects of the variation in the delay times on PVS are shown in Figure 10. As it can be observed in this Figure:

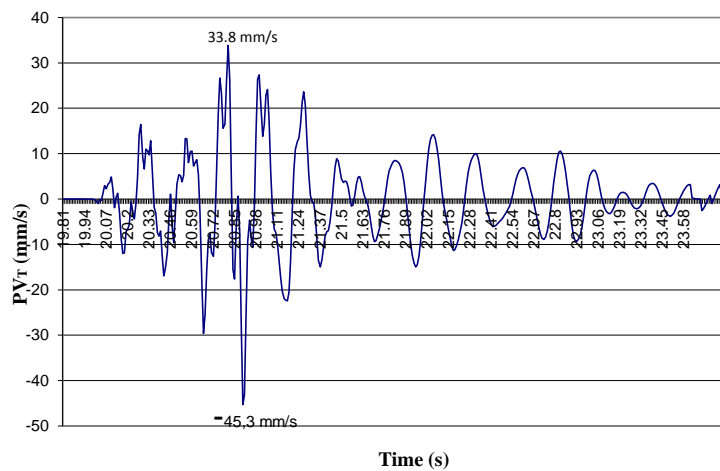- For most of the blasts, the minimum PVS was produced for a time delay of more than 40 ms.

- Among the time delays studied, the time delays 60 and 70 ms showed less level of vibration amplitude.
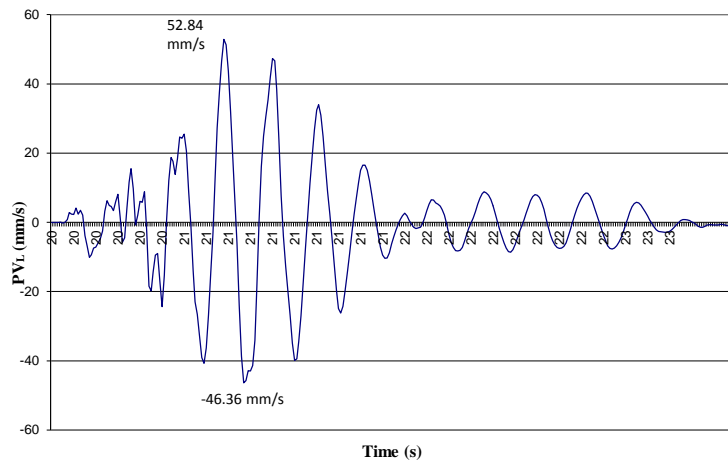
(a)
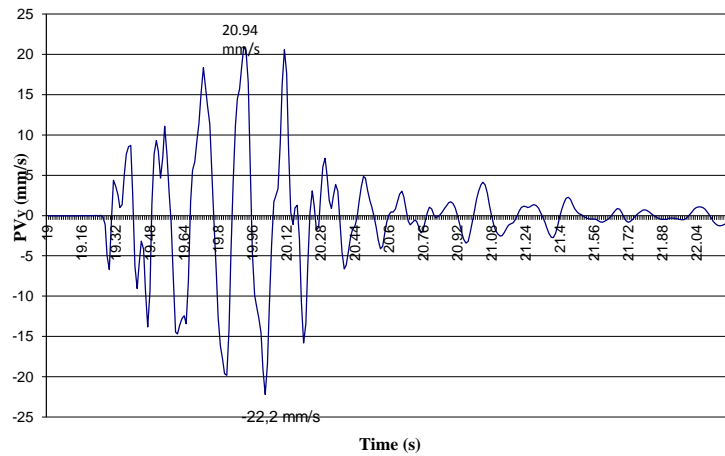
(b)

(c)

Figure 9. Synthetic seismograms of a production blast at point 8 with a delay time of 60 ms between rows. (a) longitudinal component, (b) vertical component, and (c) transversal component.
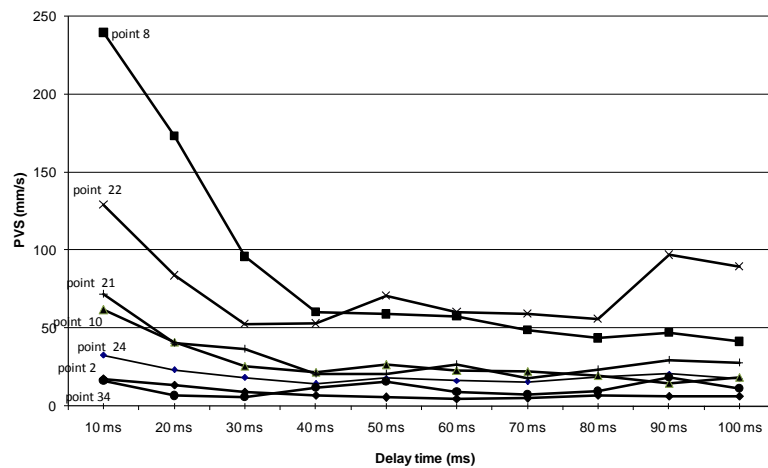
138

Figure 10. PVS *vs*. delay time at different points.

7. Conclusions

In this work, the linear superposition method was used to simulate, predict, and optimize the blast vibrations in Sar Cheshmeh copper mine. For this purpose, a linear superposition of the seismic effects of the individual holes in the blast, and also similarity of the signature seismic of the individual holes was assumed.

One single-hole blast for modeling and two double-hole blasts with the delay times of 25 and 65 ms between two holes for modeling validation were carried out. The generated vibrations were measured at seven points with different distances and directions around the blasts. Totally, 40 seismograms were synthesized (three components for each point) for two blasts using the linear superposition method. The results obtained present a good correlation between the synthetic and measured seismograms. A comparison was made between the measured PPVs and those obtained from the scaled-distance method and the linear superposition modeling, showing the merits of the linear superposition modeling over the scaled-distance method to predict PPVs. Concerning the frequency content of the measured and synthetic seismograms using the linear superposition method, strong agreements were observed between the simulated and measured frequency spectra. Also, by a systematic variation of firing delay in the modeling procedure, the effect of the delay time on the production blast vibrations was studied. The production blast simulations showed that for the Sar-Cheshmeh copper mine, the blasts with the inter-row delay times more than 40 ms can significantly reduce the vibration levels.

References

[1]. Mulay, J.M. and Ramesh, C.K. (1977). Analysis of propagation of shock-waves by finite element method. Proceedings of the 6th World Conference on Earthquake, New Delhi, India.

[2]. Siskind, D.E., Staggs, M.S., Kopp, J. and Dowding, C. (1980). Structural response and damage produced by ground vibration from surface mine blasting, USMBRI 8507.

[3]. Anderson, D., Winser, S.R. and Ritter, A. (1982). Blast design for optimizing fragmentation while controlling frequency of ground vibration. Proceedings of the Eight Conference on Explosives and Blasting Technique, Society of Explosive Engineers, Annual Meeting, New Orleans, Louisiana, USA.

[4]. Gosh, A. and Daemen, J.J.K. (1983). A simple new blast vibration predictor based on wave propagation low. 24th US Symposium on Rock Mechanics, pp. 151-161.

[5]. Harries, G. (1983).The modeling of long cylindrical charges of explosive. Proceedings of the First International Symposium on Rock Fragmentation by Blasting, Lulea, Sweden.

[6]. Shoop, S.A. and Daemen, J.J.K. (1984). Site-specific prediction of ground vibrations induced by blasting. Transaction of Society of Mining Engineers of AIME, 276: 1922-1930.

[7]. Taqieddin, S.A. (1986). Ground vibration levels: prediction and parameters. Mining Science and Technology, 3: 111-115.

[8]. Gupta, R.N., Roy, P.P., Bagchi, A. and Singh, B. (1987). Dynamics effects in various rock mass and their predictions. Journal of Mines, Metals and Fuels, 455-462.

[9]. Roy, P.P., Gupta, R.N. and Singh, B. (1989). Some recent work in analytical, empirical and statistical modeling in blasting research at CMRS India.

Proceedings of 23rd International Conference of Safety in Mines Research Institutes, Washington DC, USA.

[10]. Roy, P.P. (1993). Putting ground vibration predictions into practice. The Colliery Guardian 241 (2): 463-467

[11]. Jiang, J. (1993). Vibrations due to a buried explosive source. PhD thesis, Western Australian School of Mines.

[12]. Devine, J.F., Beck, R.H., Meyer, A.V.C. and Duvall, W.J. (1996). Effect of charge weight on vibration levels from quarry blasts. USBM RI, 6774, 37 P.

[13]. Chapot, P. (1998). Loi experimentale de propagation des vibrations dues aux tirs d'explosifs. Revue française de Géotechnique, 14 bis: 109-113.

[14]. Hirai, Y., Yamada, M., Kunimatsu, S., Durucan, S., Farsangi, M.A. and Johnston, G. J. (1998). A comparative study on numerical simulation methods used for the prediction of blast vibration. Proceedings of the 5th International Symposium on Environmental Issues and Waste Management in Energy and Material Production-SWEMO 98, Ankara, Turkey: 167-171.

[15]. Blair, D.P. (1999). Statistical model for ground vibration and air blast. Int J for Blasting and Frag. 3: 335-364.

[16]. Khandelwal, M., Singh, T.N. and Kumar, S. (2005). Prediction of blast induced ground vibration in opencast mine by artificial neural network. Indian Min Eng J 44: 23-29.

[17]. Khandelwal, M. and Singh, T.N. (2006). Prediction of blast induced ground vibrations and frequency in open cast mine- a neural network approach. J of Sound and Vib 289: 711-725.

[18]. Mohamed, M.T. (2009). Artificial neural network for prediction and control of blasting vibrations in Assiut (Egypt) limestone quarry.Int J of Rock Mech and Min Sci 46: 426-431.

[19]. Khandelwal, M. and Singh, T.N. (2009). Prediction of blast induced ground vibrations using artificial neural network. Int J of Rock Mech and Min Sci 46: 1214-1222.

[20]. Bakhshandeh Amnieh, H., Mozdianfard, M.R. and Siamaki, A. (2009). Predicting of blasting vibrations in Sar Cheshmeh copper mine by neural network, Journal of Safety Sci 48 (3): 319-325.

[21]. Monjezi, M., Ghafurikalajahi, M. and Bahrami A. (2010). Prediction of blast-induced ground vibration using artificial neural networks. Tunneling and Underground Space Tech 26 (1): 46-50.

[22]. Khandelwal, M., Kankar, P.K. and Harsha, S.P. (2010). Evaluation and prediction of blast induced ground vibration using support vector machine. Min Sci and Tech 20: 64-70.

[23]. Khandelwal, M. (2010). Evaluation and prediction of blast induced ground vibration using support vector machine. Int J of Rock Mech and Min Sci 47: 509-516.

[24]. Dowding, Ch. (1998). Construction vibration. Prentice Hall, Upper Saddle River.

[25]. Hinzen, K. G. (1988). Modeling of blast vibrations. Int J of Rock Mech and Min Sci and Geomech Abstracts, 25 (6): 439-445.

[26]. Monjezi, M., Hasanipanah, M. and Khandelwal, M. (2013). Evaluation and prediction of blast-induced ground vibration at Shur River Dam, Iran, by artificial neural network. Neural Computing and Applications 22 (7-8): 1637-1643.

[27]. Saadat, M., Khandelwal, M. and Monjezi, M. (2014). An ANN-based approach to predict blast-induced ground vibration of Gol-E-Gohar iron ore mine, Iran. Journal of Rock Mechanics and Geotechnical Engineering 6: 67-76

[28]. Yamaguchi, T., Sasaoka, T., Shimada, H., Hamanaka, A., Matsui, K., Wahyudi, S., Tanaka, H. and Kubota, S. (2014). Study on the Propagation of Blast-Induced Ground Vibration and Its Control Measure in Open Pit Mine. Mine Planning and Equipment Selection, pp. 979- 986

[29]. Anderson, D.A., Ritter, A.P. and Winzer, S. R. (1985). A method for site-specific prediction and control of ground vibration from blasting. Proceeding of the 11th ISEE Annual Conference of Explosives and Blasting Techniques, San Diego, CA, USA.

[30]. Aki, K. and Richard, P. (1980). Quantitative seismology-theory and methods, Freeman, San Francisco.

[31]. Kennett, B.L.N. and Harding, A.J. (1983). Is ray theory adequate for reflection seismic modeling?, First Break 3: 9-14.

[32]. Stump, B.W. and Reinke, R.E. (1983). Experimental confirmation of superposition from small-scale explosions. Bulletin of the Seismological Soc America 78 (3): 1059-1073.

[33]. Blair, D.P. (2008). Non-linear superposition models of blast vibration. International Journal of Rock Mech and Min Sci 45: 235-247.

[34]. Blair, D.P. and Minchinton, A. (2006). Near-field blast vibration models. Proceedings of the 8th International Symposium of Rock Fragmentation by Blasting, Chile: 152-159.

[35]. Shearer, P.M. (2009). Introduction to seismology. Cambridge University Press.

[36]. Mansouri, H. (2000). Contribution a l'analyse des effets des tirs d'abattage. Mines de sar chesmeh (Iran). PhD Thesis, ENSMP, 183 P.

مدل‌سازی لرزه‌های ناشی از انفجار با روش برهم‌نهی خطی

حمید منصوری* و محمدعلی ابراهیمی فرسنگی

بخش مهندسی معدن، دانشگاه شهید باهنر کرمان، ایران

* نویسنده مسئول مکاتبات: hmansouri@uk.ac.ir

چکیده:

به‌منظور مدل‌سازی تاریخچه زمانی لرزه‌های ناشی از انفجارهای تولیدی و بهینه‌سازی زمان‌بندی انفجار در معـدن مـس سرچشـمه، روش بـرهم‌نهـی خطـی مـورد استفاده قرار گرفت. یک انفجار تک چالی بـرای مـدل‌سـازی و دو انفجـار دو چـالی بـا تأخیرهـای بـین چـال معـادل ۲۵ و ۶۵ میلـی‌ثانیـه بـرای اعتبـار سـنجی مدل‌سازی انجام شد. لرزه‌های تولیدی در هفت نقطه اطراف نقطه انفجار با فواصل و جهت‌های مختلف اندازه‌گیری شدند. این اندازه‌گیری‌ها حاوی اطلاعـاتی در خصـوص مکانیسم پیچیده انتشار موج لرزه‌ای ناشی از انفجار و همچنین تأثیر فیلترینگ ناشی از مسیر انتشار موج است. در کـل ۴۰ سیسـموگرام بـرای دو انفجـار بـا روش برهم‌نهی خطی تولید شدند (۳ مؤلفه برای هر نقطه). نتایج به‌دست‌آمده یک همبستگی خوبی بین سیسموگرام‌های مدل‌سازی شده و انـدازه‌گیـری شـده را نشـان می‌دهد. همچنین سرعت‌های ذره‌ای اندازه‌گیری شده و به‌دست‌آمده از روش فاصله مقیاس شده و روش برهم‌نهی خطی با هم مقایسه شدند. ایـن نشـان از توانـایی روش برهم‌نهی خطی برای تخمین سرعت ذره‌ای دارد. علاوه بر آن، برای مدل‌سازی لرزه‌های یک انفجار تولیدی، سیسموگرام‌های ثبت‌شده برای انفجار تـک چـالی در هفت نقطه مورد استفاده قرار گرفتند. همچنین با تغییر سامانمند تأخیر بین ردیف‌ها در فرآیند مدل‌سازی، تأثیر تأخیر بر لرزه‌های تولیدی مورد مطالعـه قرار گرفت. مدل‌سازی‌های انفجار تولیدی نشان دادند که برای انفجارهای معدن مس سرچشمه، تأخیر بین ردیفی بیشتر از ۴۰ میلی‌ثانیه می‌تواند به‌طور معنـاداری میزان لرزه‌های تولیدی را کاهش دهد.

کلمات کلیدی: مدل‌سازی لرزه، روش برهم‌نهی خطی، سرعت حداکثر ذره‌ای، معدن مس سرچشمه.